INTERNATIONAL JOURNAL FOR NUMERICAL METHODS IN FLUIDS, VOL. 10, 161–178 (1990)

A COMPOSITE GRID APPROACH FOR THE EULER EQUATIONS

MARCELO REGGIO, JEAN-YVES TREPANIER AND RICARDO CAMARERO

Department of Applied Mathematics, Ecole Polytechnique de Montréal, PO Box 6079, Stn A, Montréal, Canada H3C 3A7

SUMMARY

A zonal grid methodology has been developed for the calculation of compressible fluid flows. The domain subdivision is based on patched grid systems composed of zones or blocks within which a distinct curvilinear grid is generated. The flow simulation is then carried out with a modified scheme based on the Euler finite volume solver of Ni. This scheme uses a distribution procedure that provides an easy and accurate way for the transfer of information from one block to another. This method results in a naturally conservative computation at the interfaces. It is analysed and developed for the treatment of embedded grids with a grid point common to more than four blocks.

KEY WORDS Euler equations Finite volumes Cell vertex storage Zonal approach

1. INTRODUCTION

The numerical simulation of flow phenomena within geometries of practical interest poses particular problems concerning the discretization of the calculation domain. In many situations the use of a single body-conforming co-ordinate system applied to the entire region allows a simple treatment of this problem. However, for complex geometries this approach can lead to an inadequate mesh, and for certain topologies the mesh cannot even be constructed.

A plausible alternative to resolve these difficulties is the use of a zonal technique. Essentially it consists of dividing a geometrically complex domain into a set of simple basic regions or zones, within each of which a grid is generated.

The implementation of the zonal grid methodology requires a corresponding composite numerical code whereby the basic equations are solved within each zone separately. The successful solution of the entire flow field by this piecewise approach depends on an adequate procedure for the transfer of the information among neighbouring blocks, and also on the manner in which the flow variables are matched at dividing boundaries. This can be done in several ways depending on the nature and degree of overlap at the zone interfaces.

In general one can distinguish two main classes of zonal approaches: overlapping grid systems (Figure 1(a)) and patched grid systems. This latter category can in turn be subdivided into point-continuous (Figure 1(b)) and point-discontinuous systems (Figure 1(c)).

The overlapping grid concept is attractive in the sense that neighbouring zones do not need to match strictly or even be similarly aligned; consequently completely differently orientated systems such as H- and O-type grids can be mixed for the solution of a given problem. However, the communication among the different zones requires the use of interpolation which may not be

0271–2091/90/020161–18$09.00

Received 19 January 1988
Revised 1 April 1989

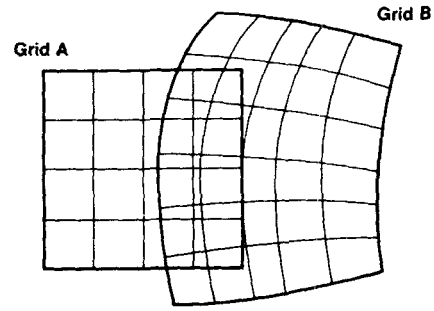

Figure 1(a). Overlapping grids

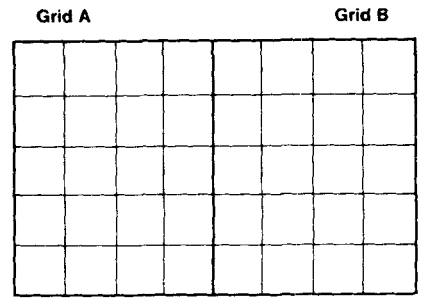

Figure 1(b). Point-continuous patched grids

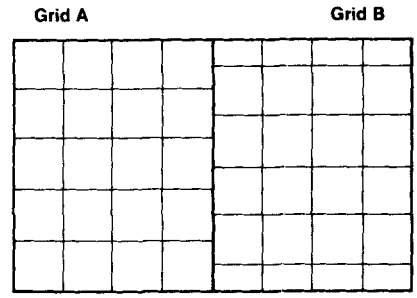

Figure 1(c). Point-discontinuous patched grids

conservative.[1,2] Applications to the solution of the full potential equation using overlapping grids have been presented in Reference 3 and 4. In Reference 4 a mass correction is introduced to reduce the error in the interzonal information exchange.

The point-continuous patched grid system is characterized by grid line continuity (but not necessarily metric continuity) across the interfaces. This implies that the grid within each zone has a certain degree of dependence with respect to its contiguous blocks, but has the interesting feature of providing a computation without any interpolation. Consequently it remains consistent with the conservation laws. Norton *et al.*[5] have applied this methodology to the computation of cascade flows. Rai *et al.*[6] present results including the supersonic flow over a cylinder with discontinuous metric across the interfaces.

The point-discontinuous patched grid system only requires that neighbouring zones meet along a common boundary. A conservative method for the solution of two-dimensional Euler equations was introduced by Rai.[7] This procedure, which treats the zonal boundary conditions together with the inclusion of local grid refinement, has since been extended to three-dimensional flow calculations by Hessenius.[8] Along other lines, Baker *et al.*[9] and Berger and Jameson[10] have also used point-discontinuous procedures when solving the Euler equations.

2. ZONAL APPROACH AND SPECIAL POINTS

The motivation for the zonal methodology is the study of a class of compressible discharge flows of intricate internal geometries with complex interactions. Ductings like the one illustrated in Figure 2 clearly cannot be discretized by the use of a single mesh, and a composite grid structure is required to accomplish such a task. When applying this approach, and depending on the organization of the basic subdomains, special points with entirely separate co-ordinate lines and directions from one zone to another[11] may arise. In such cases, and when using a standard control volume approach, particular procedures have to be implemented for the management of these specific points.

The objective of this study is to explore an extension of the Ni scheme[12] related to the interzonal coupling, using a point-continuous patched grid approach. In addition, a technique for handling the special points which arise from the zoning of special topologies is presented. The reasons for the choice of this scheme over other control volume methods are based on its high computational efficiency associated with a multiple-grid acceleration technique, and on its singular distribution technique whereby corrections to the primary variables computed at the centre of the control volumes are distributed to their corners. This attractive feature allows a simple and, more importantly, conservative manner for the interface treatment. Furthermore, a straightforward extension to imbricate four or *more* subregions at a common point *without* a special treatment is possible.

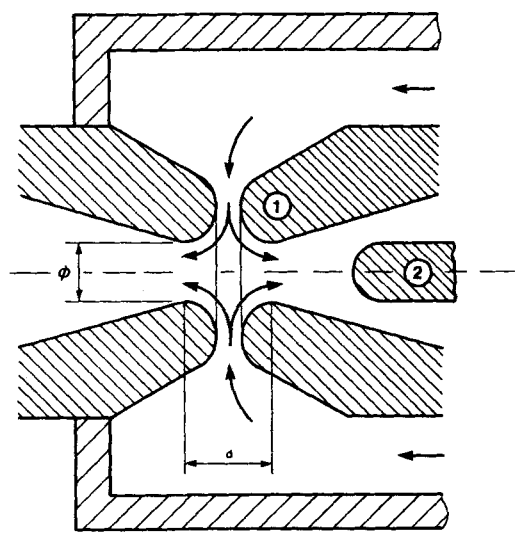

Figure 2. View of the arc chamber from Graf:[17] 1, nozzle; 2, electrode; $d = 32$ mm, $\phi = 20$ mm

Another important characteristic explored within the present framework is the use of different grid refinements on different zones. This results in point discontinuity, and care has been taken to respect conservation. In a slightly different context, related to the multigrid procedure rather than the zonal approach, Usab and Murman[13] and Dannenhoffer and Baron[14] have presented interesting alternatives to local grid refinement.

The discretization within each zone is carried out by a transfinite interpolation followed by the body-fitted grid generation method[15,16] to obtain a smooth grid.

3. GOVERNING EQUATIONS

The flows considered in the present study are governed by the conservation of mass, momentum and energy. For the unsteady state the basic equations can be written in curvilinear co-ordinates ξ, η as

$$\frac{\partial \mathbf{q}}{\partial t} + \frac{\partial \mathbf{E}}{\partial \xi} + \frac{\partial \mathbf{F}}{\partial \eta} = 0. \tag{1}$$

The flux vectors in equation (1) are defined as

$$\mathbf{q} = J\begin{bmatrix} \rho \\ \rho u \\ \rho v \\ e \end{bmatrix}, \quad \mathbf{E} = J\begin{bmatrix} \rho U \\ \rho u U + p\xi_x \\ \rho v U + p\xi_y \\ (e+p)U \end{bmatrix}, \quad \mathbf{F} = J\begin{bmatrix} \rho V \\ \rho u V + p\eta_x \\ \rho v V + p\eta_y \\ (e+p)V \end{bmatrix},$$

where the terms ξ_x, ξ_y, η_x, η_y represent the metrics and J is the Jacobian. In this formulation there are two sets of velocities. The curvilinear velocity components U, V and the Cartesian velocity components u, v, are related by

$$U = u\xi_x + v\xi_y, \qquad V = u\eta_x + v\eta_y. \tag{2}$$

4. NUMERICAL SCHEME

The solution method for the Euler equations (equation (1)) is based on Ni's scheme[12] coupled with a multigrid acceleration technique. The scheme can be derived by first approximating the temporal correction of the primary variables using the following Taylor series expansion:

$$\mathbf{q}(t+\Delta t) - \mathbf{q}(t) = \mathbf{q}_t \Delta t + \mathbf{q}_{tt}\frac{\Delta t^2}{2} + O(\Delta t^3). \tag{3}$$

Using equation (1), the time derivatives appearing in this relation can be expressed in terms of space derivatives as

$$\mathbf{q}_t = -(\mathbf{E}_\xi + \mathbf{F}_\eta), \qquad \mathbf{q}_{tt} = [\mathbf{A}(\mathbf{E}_\xi + \mathbf{F}_\eta)]_\xi + [\mathbf{B}(\mathbf{E}_\xi + \mathbf{F}_\eta)]_\eta,$$

where

$$\mathbf{A} = \frac{\partial \mathbf{E}}{\partial \mathbf{q}}, \qquad \mathbf{B} = \frac{\partial \mathbf{F}}{\partial \mathbf{q}}. \tag{4}$$

Substituting into equation (3) yields the following expression for the variable increment in time:

$$\delta\mathbf{q} = -\Delta t(\mathbf{E}_\xi + \mathbf{F}_\eta) + \frac{\Delta t^2}{2}\{[\mathbf{A}(\mathbf{E}_\xi + \mathbf{F}_\eta)]_\xi + [\mathbf{B}(\mathbf{E}_\xi + \mathbf{F}_\eta)]_\eta\}. \tag{5}$$

The finite volume approximation of this equation can be carried out by using the information given by a nine-node computational cell (Figure 3) resulting from the assembly of the four basic subcells A, B, C and D. This step plays a key role related to the conservation principle which is now detailed.

Let us define Δq_A, Δq_B, Δq_C and Δq_D as the first-order changes in the basic subcells. The change Δq in a subcell, say for example C, is given by

$$\Delta \mathbf{q}_C = \frac{\Delta t}{2V_C}\{[(\mathbf{E}_P + \mathbf{E}_N) - (\mathbf{E}_E + \mathbf{E}_{NE})]\Delta\eta + [(\mathbf{F}_P + \mathbf{F}_E) - (\mathbf{F}_N + \mathbf{F}_{NE})]\Delta\xi\}, \tag{6}$$

where the subscripts are defined in Figure 3.

In order to obtain the change at point P, these four increments have to be assembled. In the proposed approach, this assembly is performed on the basis of a secondary (or dual) cell associated with the node P, whose definition is now explained.

A typical subcell (Figure 4) is first subdivided into four control subvolumes with internal boundaries defined by co-ordinate lines joining the midpoints of opposite sides. The intersection

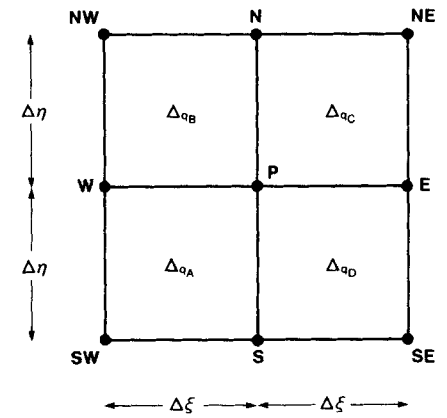

Figure 3. Nine-node computational cell and basic subcells

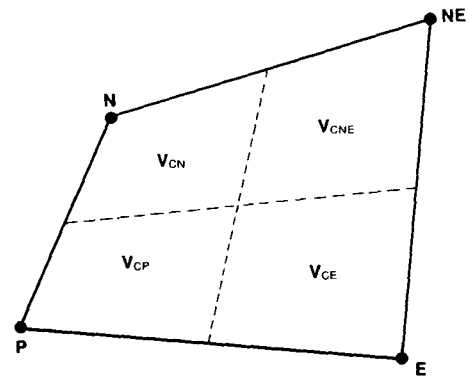

Figure 4. Subdivision of subcell C into four control sub-volumes

of these lines specifies the (x^*, y^*) geometric centre of the cell, which can also be seen as the averaging of the four (x, y) nodal values of the cell. This choice for subdivision implies a symmetric distribution of the subcontrol volume edges, but *not* an equal volume partition.

Once the subcontrol volumes are defined, these are assembled at a common node and the dual cell is generated. This element contains four control subvolumes from four different primary cells, thus being described by eight line segments, two in each of the cells A, B, C and D. This idea is illustrated in Figure 5.

The reason for this choice, instead of using the original cell (Figure 3), is that in such a case, characterized by an even distribution of the changes on a cell to its vertices, the whole increment in a subcell is used in the assembly of four different points, and an overlapping occurs (Figure 6). This implies that conservation is not strictly assured.

In contrast, when the assembly is carried out on the displaced cells (Figure 5), there is no such overlapping, and a fully conservative scheme consistent with the basic principle of finite volumes,

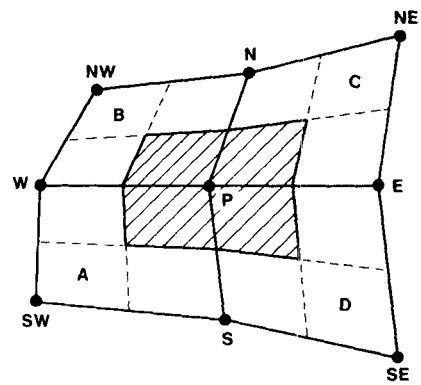

Figure 5. Assembled dual cell

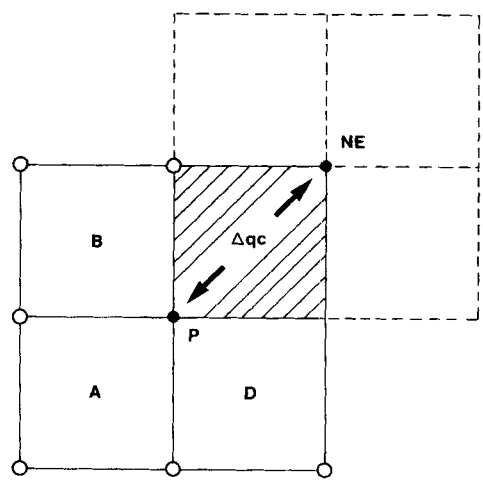

Figure 6. Contribution of $\Delta \mathbf{q}_C$ to the P and NE nodes

with fluxes at element edges cancelling each other, results. In this manner, all conservation laws are applied to the same control volume, there being one control volume associated with each point.

In order to accomplish this operation, the changes calculated by equation (6) are first weighted by the portion of the volume of the basic subcells related to the node P (V_{CP} in Figure 4). In general, these fractions are not a quarter of the volume of the subcells. Then the summation of these volume-weighted changes is averaged by the volume of the secondary cell,

$$V_P = V_{AP} + V_{BP} + V_{CP} + V_{DP}.$$

In doing so, the leading term of (5) (the first-order change in time) can be represented by the following discrete form:

$$\Delta \mathbf{q}_P = \frac{1}{V_P}[\Delta \mathbf{q}_A V_{AP} + \Delta \mathbf{q}_B V_{BP} + \Delta \mathbf{q}_C V_{CP} + \Delta \mathbf{q}_D V_{DP}]. \tag{7}$$

This practice for computing the first-order changes can be regarded as a conservative transfer from the primary grid (Figure 3) to the dual mesh (Figure 5). It should be noted that using a Cartesian mesh, and if the volumes of the four basic sub-cells are equal, the present method coincides with the distribution procedure introduced by Ni,[12] i.e.

$$\Delta \mathbf{q}_P = \tfrac{1}{4}(\Delta \mathbf{q}_A + \Delta \mathbf{q}_B + \Delta \mathbf{q}_C + \Delta \mathbf{q}_D).$$

With the first-order changes in time now in hand, we turn to the second-order term. Consistent with Ni, expressions such as the following can be defined at the centre of the different subcells:

$$\Delta \mathbf{E}_C = \mathbf{A}_C \Delta \mathbf{q}_C, \qquad \Delta \mathbf{F}_C = \mathbf{B}_C \Delta \mathbf{q}_C, \tag{8}$$

where **A** and **B** are the Jacobian matrices defined by equations (4). Using these, the second-order changes in time (i.e. the second term of equation (5)) can be approximated as follows:

$$\frac{\Delta t}{2}\{[\mathbf{A}\Delta t(\mathbf{E}_\xi + \mathbf{F}_\eta)]_\xi + [\mathbf{B}\Delta t(\mathbf{E}_\xi + \mathbf{F}_\eta)]_\eta\} = -\frac{\Delta t}{2}\{[\mathbf{A}\Delta \mathbf{q}]_\xi + [\mathbf{B}\Delta \mathbf{q}]_\eta\} = -\frac{\Delta t}{2}(\Delta \mathbf{E}_\xi + \Delta \mathbf{F}_\eta).$$

Applying the control volume approximation of these changes on the secondary cells, the following discretization is obtained:

$$\frac{\Delta t}{4V_P}[(\Delta \mathbf{E}_A + \Delta \mathbf{E}_B)\Delta\eta - (\Delta \mathbf{E}_C + \Delta \mathbf{E}_D)\Delta\eta + (\Delta \mathbf{F}_A + \Delta \mathbf{F}_D)\Delta\xi - (\Delta \mathbf{F}_B + \Delta \mathbf{F}_C)\Delta\xi]. \tag{9}$$

Combining equation (5), (6) and (8) yields an expression for the overall correction to the conservation variables:

$$\delta \mathbf{q}_P = \frac{1}{V_P}[\Delta \mathbf{q} V_{AP} + \Delta t(\Delta \mathbf{E}^* + \Delta \mathbf{F}^*)]_A + \frac{1}{V_P}[\Delta \mathbf{q} V_{BP} + \Delta t(\Delta \mathbf{E}^* - \Delta \mathbf{F}^*)]_B$$
$$+ \frac{1}{V_P}[\Delta \mathbf{q} V_{CP} + \Delta t(-\Delta \mathbf{E}^* - \Delta \mathbf{F}^*)]_C + \frac{1}{V_P}[\Delta \mathbf{q} V_{DP} + \Delta t(-\Delta \mathbf{E}^* + \Delta \mathbf{F}^*)]_D, \tag{10}$$

where the superscript star is used to denote fluxes across the faces of the dual elements.

The structure of equation (10) may be interpreted as a formula that distributes first-order changes $\Delta \mathbf{q}$ and second-order changes $\Delta \mathbf{E}$ and $\Delta \mathbf{F}$ to the vertices of the primary cells.

Thus the global correction procedure can be summarized by the following sequence:

1. The first-order changes in the subcells A, B, C and D are calculated according to equation (6).
2. The second-order changes are computed using equations (8).

3. The first- and second-order changes are distributed according to equation (10).
4. The dependent variable $\mathbf{q}$ is updated by

$$\mathbf{q}^{n+1} = \mathbf{q}^n + \delta\mathbf{q}.$$

5. MULTIPLE-GRID PROCEDURE

The convergence of the above basic algorithm can be substantially improved by using a multiple-grid procedure proposed by Ni[12]. Essentially it consists of effectively propagating the corrections given by equation (10) throughout the calculation domain by using successively coarser grids. This allows a larger time step, thus accelerating the convergence. Details concerning the multigrid algorithm can be found in References 12, 17 and 18.

6. ZONAL DISCRETIZATION

A valuable discretization tool currently employed in grid generation is the body-conforming technique.[15] In its basic form, this procedure yields a curvilinear mesh on a single region bounded by two pairs of opposite curves, in such a manner that co-ordinate lines are coincident with the respective domain boundaries.

The generalization of this idea to more complex domains such as a multibranched channel passage, where the topology is no longer represented by a four-sided domain, can lead to a cumbersome grid generation process, which complicates the subsequent flow simulation. A good strategy to overcome these difficulties is the zonal grid methodology. According to this, the physical field is first segmented into a number of contiguous subdomains, each of them with the general form of a curved-sided quadrilateral and logically treated as a rectangle. Once the zones are defined, their boundaries are discretized by applying a linear interpolation procedure. Using this boundary point distribution, the distinct subdomains are initially gridded by using a transfinite interpolation. This mesh can be subsequently smoothed by solving an elliptic system[15] (i.e. turned into a body-fitted grid). It is at this stage that partial or complete continuity of grid lines between blocks is obtained as a result of the interface treatment. In fact, since the interfaces are not actual boundaries, these can be considered as interior elements and calculated using values of the points on surrounding layers outside the zone. This allows the points on an interface to move freely, with their final location determined by the grid generation procedure. In this case complete continuity is achieved. Alternatively, the points at the interface location may be completely specified (as for real boundaries). In this instance the points common to two joining blocks and originally defined from the interpolation procedure do not move, and only point (but no slope) continuity results.

7. BOUNDARY CONDITIONS AND INTERFACE TREATMENT

According to the zonal method, the flow simulation on a complex region is carried out into geometrically simpler four-sided subdomains. The flow solver treats every logical block as a rectangle to which appropriate boundary conditions are applied. On a given zone, a side can be an inlet, an outlet, a solid wall or an interface. The first three types of boundaries are physical and are treated accordingly. The last type, whose location is arbitrary, is in fact a fictitious permeable interface, and no boundary condition should be applied on it. It is at this point that the Ni scheme becomes particularly interesting, because it allows a proper treatment of the zonal boundary for the governing equations.

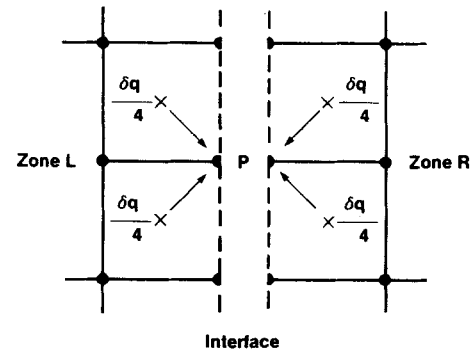

Figure 7. Change distribution to a point on an interface

The core of the method, represented by the distribution formula (10), indicates how first- and second-order corrections calculated on an element are divided to its four vertices. This characteristic renders the scheme well suited for the implementation of the zoning. For the case of a standard grid node (surrounded by eight points) at the interface of two zones, the situation can be regarded in the following way.

The node P will first receive the contribution of two interior elements of the current zone (zone L, Figure 7). This correction will be subsequently completed when treating the adjacent zone (zone R, Figure 7), which will result in two others contributions. In this manner, a point at an interface shared by two blocks is in fact treated as if it were any other interior point.

This considerably simplifies the coding, since no additional row of fictitious points or interpolation procedure is required to provide the connection across the interfaces.

8. SPECIAL POINTS

An important feature of the proposed distribution method appears in the handling of the special points, i.e. those that are not surrounded by eight neighbours. Among these we distinguish two types, those common to five (or more) subregions (Figure 8) and those at an interface between two regions of different grid density (Figure 9(a)).

In the first case the treatment is just the natural application of the assembly procedure described in Section 4. Namely, the five changes arising will be weighted by their corresponding volumes and summed, i.e. $\delta\mathbf{q}_P = \sum_{i=1}^{i=5} \delta\mathbf{q}_i \mathbf{V}_{iP}$, then this weighted correction will be averaged by the volume associated with the node P, i.e. $V_P = \Sigma_{i=1}^{i=5} V_{iP}$, yielding the actual correction $\delta\mathbf{q} = \delta\mathbf{q}_P / V_P$. If, for example, all linking elements have unit volume, this can be interpreted as if every element contributes one-fifth of the total correction to this point.

The handling of the second family of singular points (Figure 9(a)) can also be regarded in the context described in Section 4; however, this time a further explanation is presented.

A basic condition that a scheme has to respect to maintain global conservation is that all interior fluxes cancel each other. This must also be true for a zonal boundary, with any residual fluxes remaining on this. For the case of cell A illustrated in Figure 9(a), this implies that the appropriate flux balance must be carried out by considering the fluxes through its five faces 1–2, 2–4, 4–7, 7–6 and 6–1. This point on conservative flux balance for this specific configuration has been previously evoked in Reference 14.

Once this conservative flux balance is done, the question that remains is how to distribute the correction computed on cell A to its five nodes. As previously stated, this is carried out on the basis

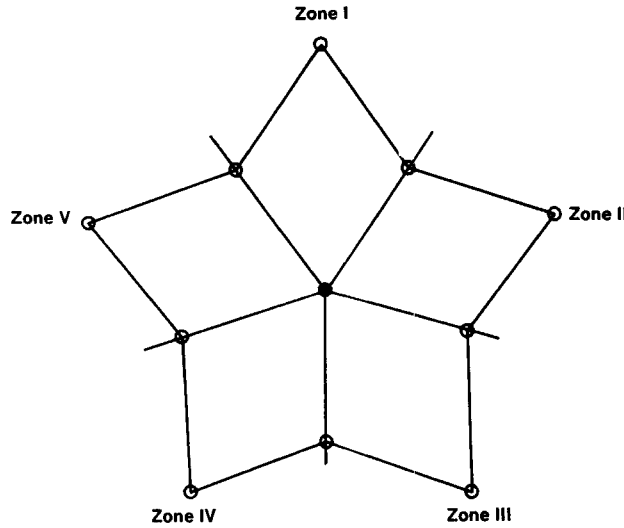

Figure 8. Star point surrounded by 10 neighbours

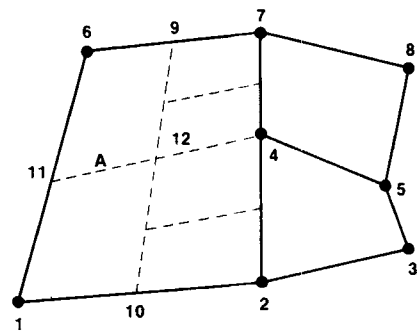

Figure 9(a). Fine and coarse mesh interfacing

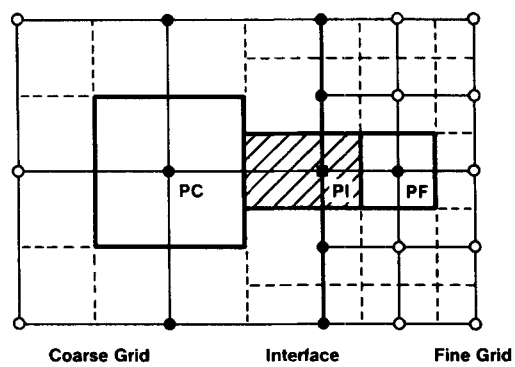

Figure 9(b). Dual cell at a fine and coarse mesh interfacing

of the dual cells. Figure 9(b) illustrates the configuration of these near and at the interfacing of the coarse and fine grids. The points PC on the coarse mesh and PF on the fine mesh correspond to internal points on the respective zones, so that the corrections to these nodes are treated via the normal assembly procedure.

The point PI is on the interface, and the correction to this node has to take into account simultaneous changes belonging to the coarse and fine meshes. These changes require the definition of associated volumes. The volumes arising from the fine mesh side and specified in the same manner as for any other regular point. For the definition of the volumes arising from the coarse mesh side we proceed as follows.

The midpoints on the 6–7 (point 9) and 1–2 (point 10) faces (Figure 9(a)) are joined, and the midpoint on the side 1–6 (point 11) and node 4 are linked. The intersection of these lines defines the point 12 (which it is not necessarily the geometric centre). Then the midpoint on the face 2–4 and a point halfway between points 10 and 12 are connected. Finally the midpoint on the face 4–7 and the midpoint on the side 12–9 are also linked. In this manner the portion of the dual cell belonging to the coarse mesh side is obtained, thus completing the definition of the peculiar element.

Regardless of the definition of the dual cell associated with node PI (Figure 9(b)), any singular treatment must follow the basic premise of any finite volume procedure, i.e. it must have a statement of conservation applied on it. This attribute was not considered in Reference 13 and 14, in which the correction to this node (point 4 in Figure 9(a)) is obtained by averaging the distribution to nodes 2 and 7. It should be noted that the proposed geometry of the transition cell is not unique. Other descriptions can be imposed, but they should always be treated so as to ensure global conservation.

In spite of the fact that the technique described above is general, caution is required in the code structure regarding the connectivity of the nodal points. The subdivision process, which is performed individually on each block, identifies a grid point with the integers I, J corresponding to logical local co-ordinates in the interior of each zone. The connection of any I, J point within a block with its immediate neighbours is simply given by the structure $I \pm 1, J$; $I, J \pm 1$. On the other hand, nodal points along block interfaces simultaneously belong to different systems and should be uniquely distinguished. When more than four zones meet at a single point, the co-ordinate system cannot be consistently followed across all the interfaces, and the 'smashing' of the $I(\xi)$ co-ordinate by a $J(\eta)$ co-ordinate (or vice versa) at some interface is unavoidable. This problem has been solved by assigning a single index to all nodes after subdividing each of the blocks. In this way all nodal points having the same co-ordinate will be represented by the same index, thus eliminating any possible ambiguity.

9. COMPUTED RESULTS

NACA0012

The current approach was first applied to the computation of the flow around the NACA0012 aerofoil at an angle of attack α of zero and for a freestream Mach number $M = 0{\cdot}8$. The discretization was carried out using an O-type grid with (160×36) mesh points.

Figure 10 compares the current prediction with the results of Reference 19 in terms of the pressure distribution. Both solutions are substantially the same, predicting equal shock position and intensity. However, a slightly sharper shock emanates from the present calculations. Near the trailing edge, the current computation displays a more pointed curve; this is attributed to fewer points being used in this region.

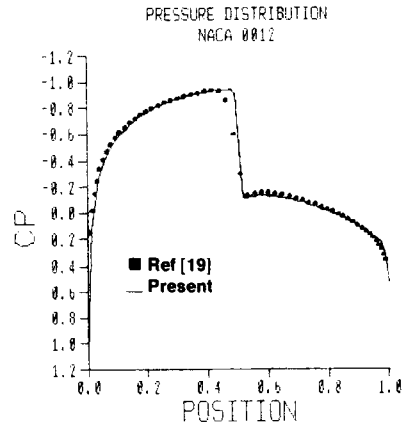

Figure 10. Comparison of calculated pressure distribution with results of Reference 19 ($M=0{\cdot}8$, $\alpha=0$)

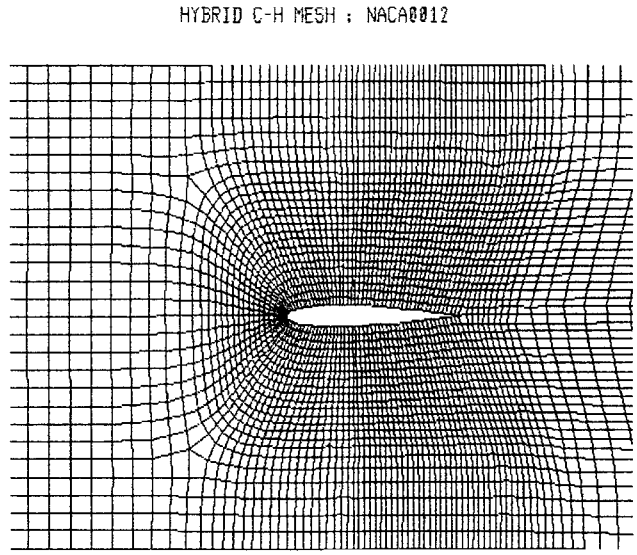

Figure 11. Embedded co-ordinate grid system with a star point

A second application of the present composite approach was carried out on a NACA0012 cascade passage. Aerofoils in the cascade are unstaggered and the pitch-to-chord ratio is 3·6. The freestream angle is zero.

A suitable grid for this type of configuration can be achieved by combining C- and H-type grids. This results in an appropriate grid for near-blade regions, where the C-type grid is employed, and in a satisfactory mesh for the upstream region, where the H-type grid is used.

A partial view of this embedded co-ordinate grid is shown in Figure 11, where a star point appears as a consequence of the composite discretization.

The transonic case for conditions leading to an inlet Mach number of 0·8 was computed. Figure 12 illustrates iso-Mach lines in the vicinity of the special star point. Close examination

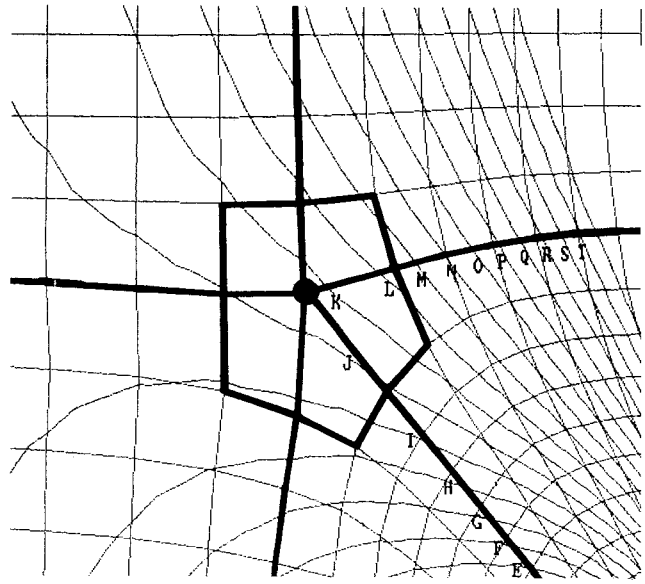

Figure 12. Iso-Mach contours near the star point

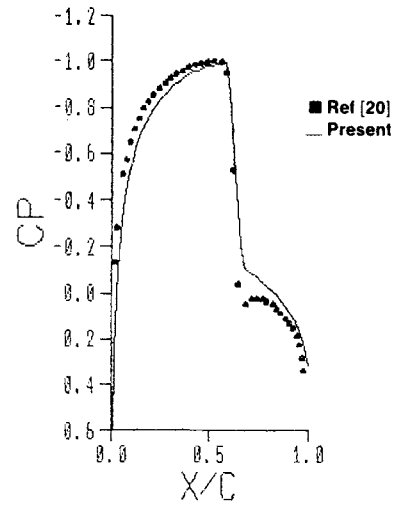

Figure 13. Pressure coefficient for a non-lifting NACA0012 cascade

shows no unrealistic behaviour of the computed fluid parameters, clearly indicating the correctness of the treatment.

The pressure coefficient was computed and is illustrated in Figure 13. The computed results agree reasonably well with those presented in Reference 20, with the exception of the maximum recovery pressure after the shock. This discrepancy could be attributed to the different models used.

JPL nozzle

With the objective of testing a second characteristic of the proposed approach, namely point discontinuity arising from different grid densities, the geometry of the nozzle studied by Cuffel *et al.*[21] was chosen to conduct a second group of tests. Because a flow in which a strong shock appears is more appropriate for the verification of a zonal reduction, the nozzle was operated at a pressure ratio $P_b/P_o = 0{\cdot}7$.

A first study was conducted by subdividing the domain into three zones, each of them with a consecutive double grid density from the inlet to the outlet. Figure 14(a) illustrates the discretization. Computation of a plane flow using this discretization predicts a shock in the finer zone near the outlet. The depicted iso-Mach lines in Figure 14(b) show continuity from one zone to an other, revealing a transparent interfacing.

A second zoning was then applied by dividing the nozzle into two regions from the axis of symmetry to the wall, with a mesh twice as fine in the upper zone. The zones and the grid are shown in Figure 15(a). In this case the shock represented by iso-Mach contours indicates bands of different thickness on each region (Figure 15(b)). This is intimately related to the mesh size, as expected. Here the transition from one region to the other is also smooth, indicating the correctness of the procedure.

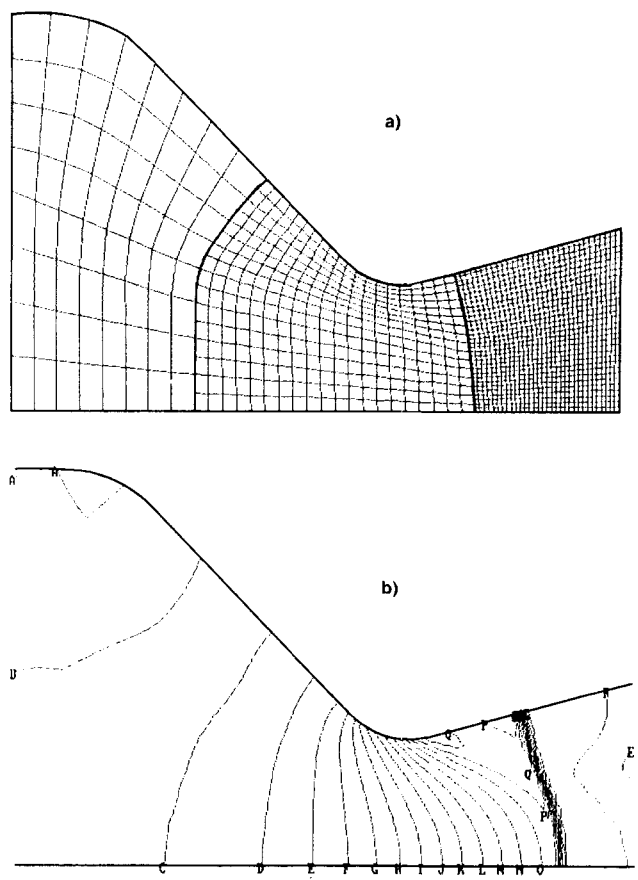

Figure 14. Composite grid and (b) iso-Mach contours for three-zone nozzle calculation

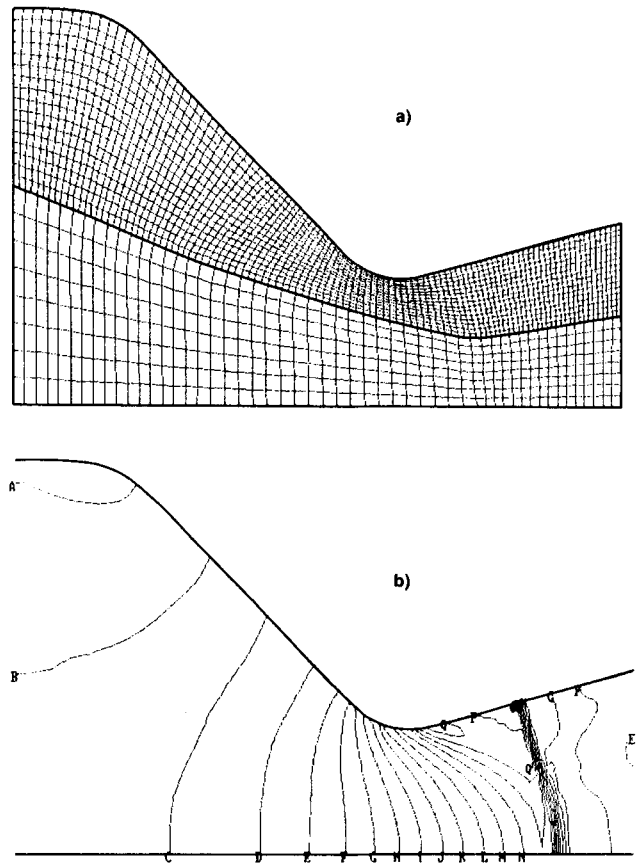

Figure 15. Composite grid and (b) iso-Mach contours for two-zone nozzle calculation

A final test was performed for this nozzle, for an axisymmetric subsonic–supersonic flow. The discretization for this test is the same that used for the first case (Figure 14(a)). Note that in order to remain coherent with the axisymmetric configuration, the weighting procedure presented in Section 4 has to include the radial co-ordinate in order to correctly represent the influence of the volumes.

The results, displayed in Figure 16 in terms of the Mach number at the wall and at the centreline, are compared with the experimental data of Reference 21. A good concordance of the numerical calculations with the measured values is encountered. Once again no discontinuity appears at the interfacing.

Double nozzle

As a last application, the current approach was used to compute a flow studied experimentally by Graf *et al.*[22] The geometry employed by these authors consists of an axisymmetric chamber with a dual-flow nozzle arrangement and an electrode (Figure 2). This type of configuration is found in circuit-breaker devices, where a discharge flow interacting with a strong electric arc takes place. The present numerical simulation was restricted to the aerodynamic aspects of the flow, neglecting the interaction with the electric arc.

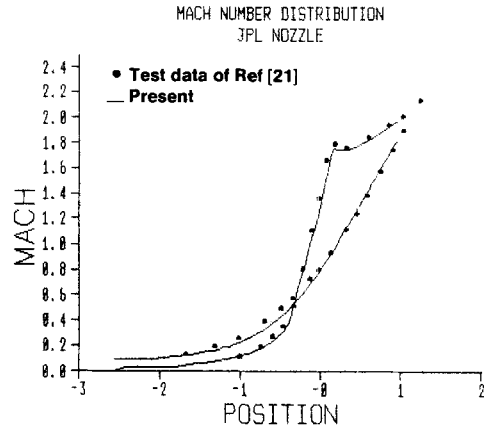

Figure 16. Comparison of JPL nozzle Mach number distribution at wall and centreline

Figure 17 illustrates the zoning, where a star point with five meeting zones can be seen. The domain was subdivided into 12 zones, and the discretization used a total of 2192 points.

The calculations made for this case reveal that the flow reaches the sonic point at the throat of the nozzle, so that when approaching the electrode on the right, a bow shock forms. Figure 18

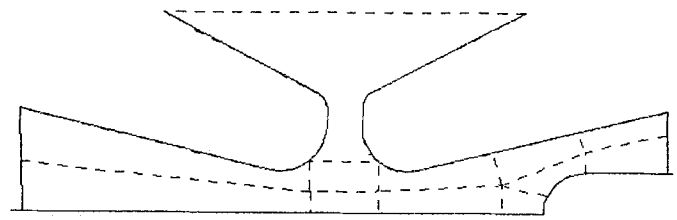

Figure 17. Zoning for the geometry of Reference 22

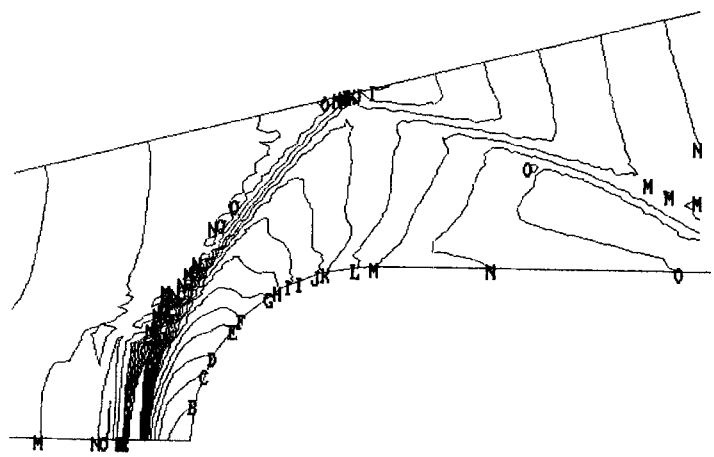

Figure 18. Computed Mach contours near the electrode

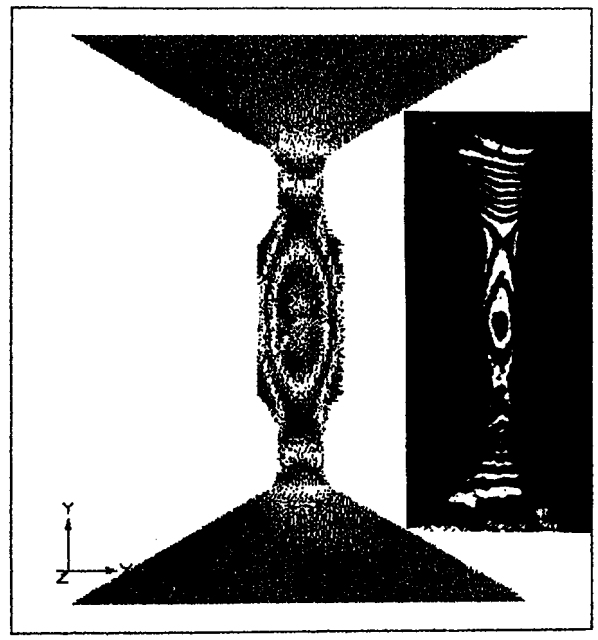

Figure 19. Comparison of numerical and experimental interferograms

shows an enlarged view of computed Mach contours near the electrode region. The flow reaches the electrode with a Mach number around 3, and a detached shock is predicted. A reflection of the shock on the outer wall of the nozzle can also be expected.

Figure 19 depicts computed contours of constant density, represented by means of a cloud of points, and compares them with the interferogram obtained in Reference 22. Although this parallel is only qualitative, the similarity is remarkable.

10. CONCLUSIONS

A zonal approach was developed and implemented for the solution of the Euler equations in multibranched geometries.

A fully conservative procedure based on the work of Ni was devised. The proposed method is characterized by a finite volume technique with one control volume associated with each grid node. The distributive or assembly nature of the scheme, together with the presented approach, allow a straightforward and conservative manner for the transfer of information from one zone to another.

Point-continuous and point-discontinuous patched grid systems were applied in various test cases. For the first type of gridding, particular points meeting more than four zones were successfully treated. For the second kind of grid configuration, the correct treatment of transition elements, which makes it possible to match one control volume with two others side-by-side, was also achieved.

REFERENCES

1. J. A. Benek, J. L. Steger and F. C. Doughtery, 'A flexible grid embedding technique with application to the Euler equations', *AIAA Paper 83-1944*, 1983.
2. K. A. Hessenius, and T. H. Pulliam, 'A zonal approach to solution of the Euler equations', *AIAA Paper 82-0969*, 1982.

3. E. H. Atta, 'Component-adaptive grid interfacing', *AIAA Paper 81-0382*, 1981.
4. C-Y Gu and L. Fuchs, 'A non-isentropic interpolation scheme applied to zonal-grid calculation of transonic flows', in C. Taylor, W. G. Habashi and M. Hafez (eds), *Proc. 5th Int. Conf. on Numerical Methods in Laminar and Turbulent Flows*, Pineridge Press, Swansea, 1987, pp. 975–986.
5. R. T. G. Norton, W. T. Thompkins and R. Haimes, 'Implicit finite difference schemes with non-simply connected grids—a novel approach', *AIAA Paper 84-003*, 1984.
6. M. M. Rai, K. A. Hessenius and S. R. Chakravarthy, 'Metric-discontinuous zonal grid calculations using the Osher scheme', *Comput. Fluids*, **12**, 161–175 (1984).
7. M. M. Rai, 'A conservative treatment of zonal boundaries for Euler equation calculations', *J. Comput. Phys.*, **62**, 472–503 (1986).
8. K. A. Hessenius, 'Conservative zonal schemes for patched grids in two and three-dimensions', *Ph.D. Dissertation*, Mechanical Engineering Department, Stanford University, 1986.
9. T. J. Baker, A. Jameson and R. E. Vermeland, 'Three-dimensional Euler solutions with grid embedding', *AIAA Paper 85-1021*, 1985.
10. M. J. Berger and A. Jameson, 'Automatic adaptive grid refinement for the Euler equations', *Proc. 9th Conf. on Numerical Methods in Fluid Dynamics*, 1984, pp. 14–16.
11. J. F. Thompson, Z. U. A. Warsi and C. W. Mastin, '*Numerical Grid Generation Foundations and Applications*', Elsevier, 1985.
12. R.-H. Ni, 'A multiple-grid scheme for solving the Euler equations', *AIAA Paper 81-1025*, 1981.
13. W. J. Usab and E. M. Murman, 'Embedded mesh solutions of the Euler equation using a multiple-grid method', *Advances in Computational Transonics*, Pineridge Press, Swansea, 1985, pp. 447–472.
14. J. F. Dannenhoffer and J. D. Baron, 'Grid adaptation for the 2-D Euler equations', *AIAA Paper 85-0484*, 1985.
15. J. F. Thompson and Z. U. Warsi, 'Boundary-fitted coordinate systems for numerical solution of partial differential equations—a review', *J. Comput. Phys.*, **7**, 1–108 (1982).
16. R. Camarero *et al.*, 'Introduction to grid generation systems in turbomachinery', *VKI Lecture Series 2, Numerical Techniques for Viscious Calculation in Turbomachinery*, 1986.
17. C. Koeck, 'Computation of three-dimensional flow using the Euler equations and a multiple-grid scheme', *Int. j. numer. method fluids*, **5**, 483–500 (1985).
18. R. Chima and G. Johnson, 'Efficient solution of the Euler and Navier Stokes equations with a vectorized multiple-grid algorithm', *AIAA J.*, **23**, 23–32 (1985).
19. A. Jameson and S. Yonn, 'Multigrid solution of the Euler equations using implicit schemes', *AIAA J.* **14**, 1737–1743 (1986).
20. C. Farrell and J. Adamczyk, 'Full potential solution of transonic quasi-three-dimensional flow through a cascade using artificial compressibility', *ASME J. Eng. Power*, **104**, 143–153 (1982).
21. R. F. Cuffel, L. H. Back and P. F. Massier, 'Transonic flowfield in a supersonic nozzle with small throat radius of curvature', *AIAA J.*, **7**, 1364–1366 (1969).
22. H. P. Graf, H. P. Meili, E. Fischer and H. J. Schoetz, 'Axially blown SF_6-arcs around current zero', *Appl. Phys. B*, **36**, 33–40 (1985)